Ultra salt-resistant solar desalination system via large-scale easy-assembly of microstructural units

Chenyang Dang[1], Hua Wang[2], Yunteng Cao[3], Jing Shen[1], Jia Zhang[1], Letian Lv[1], Guiyin Xu[1]*, Meifang Zhu[1]*

1 State Key Laboratory for Modification of Chemical Fibers and Polymer Materials, College of Materials Science and Engineering, Donghua University Shanghai 201620, China

2 Hangzhou Global Scientific and Technological Innovation Center, Zhejiang University, Hangzhou, Zhejiang 310027, China

3Department of Civil and Environmental Engineering, Massachusetts Institute of Technology, Cambridge, MA 02139, USA

Table of contents

Figure S13. Evaporation, accumulation-salt and refresh performance of SR evaporators in supersaturated brine under 5 sun irradiation.

Figure S14. Evaporation performance of SR-3mm (willow) evaporator in brine with 5wt% and 20wt% salinity under 1 sun.

Figure S15. UV-vis-NIR absorption spectra of the natural cotton and ink@cotton.

Figure S16. FTIR spectrum of the natural cotton and ink@cotton.

Figure S17. Evaporation rate of the SR evaporator (cotton) and ordinary evaporator (cotton) operating in 25wt% brine under 1 sun.

Figure S18. Optical image of the SR evaporator (cotton) and ordinary evaporator (cotton) operating in 25wt% brine under 1 sun.

Figure S19. Photothermal efficiency of the SR evaporator (cotton) and ordinary evaporator (cotton) operating in 25wt% brine under 1 sun.

Figure S20. Outdoor real-time light intensity and temperature changes.

Figure S21. Bill of materials for SDID system.
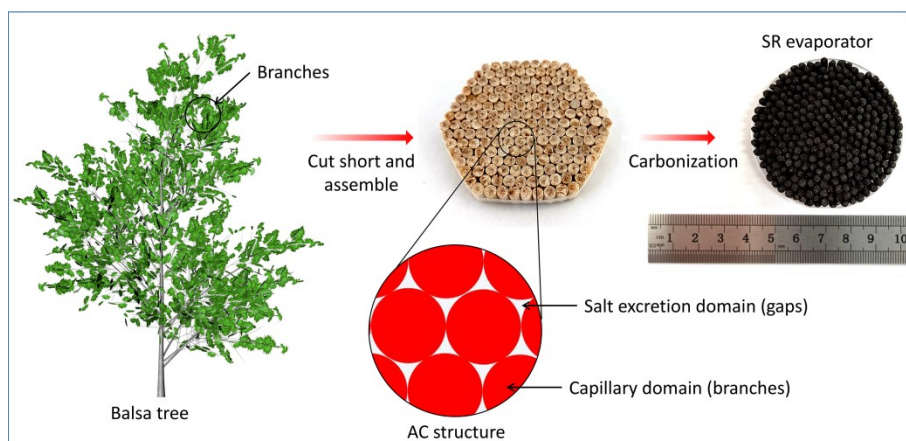
Figure S1. The tree branches are assembled to prepare PTMs with SR structure.
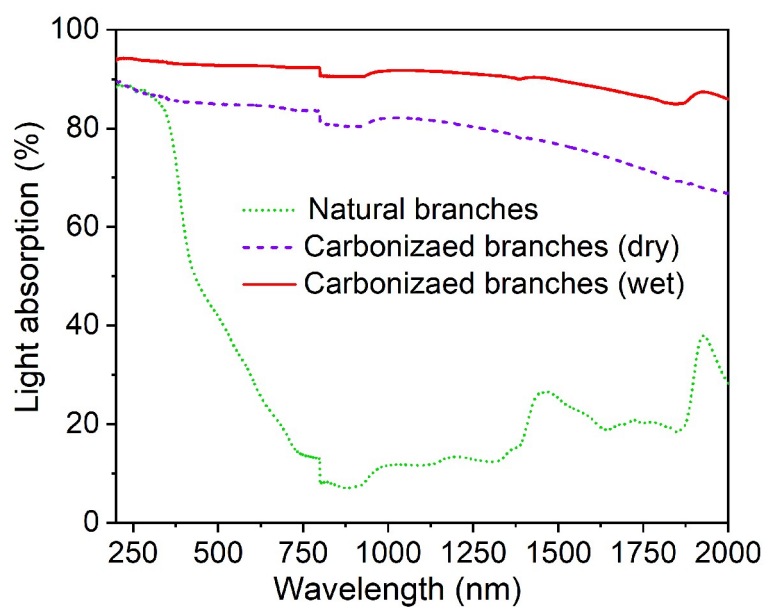
Figure S2. UV-vis-NIR absorption spectra of the natural branches and the carbonized branches.
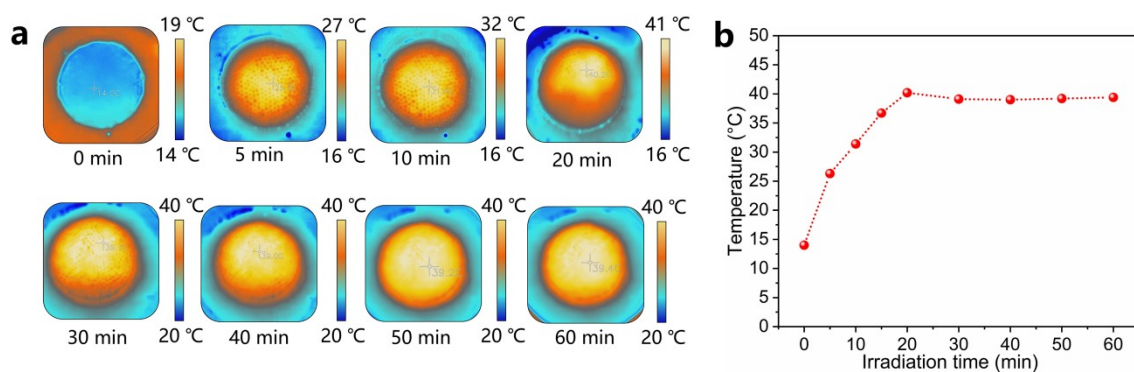
Figure S3. Photothermal response characteristics of SR-3mm evaporator. (a) Infrared photo of the temperature distribution on the surface of the SR-3mm evaporator. (b) The surface temperature of the SR-3mm evaporator over time.
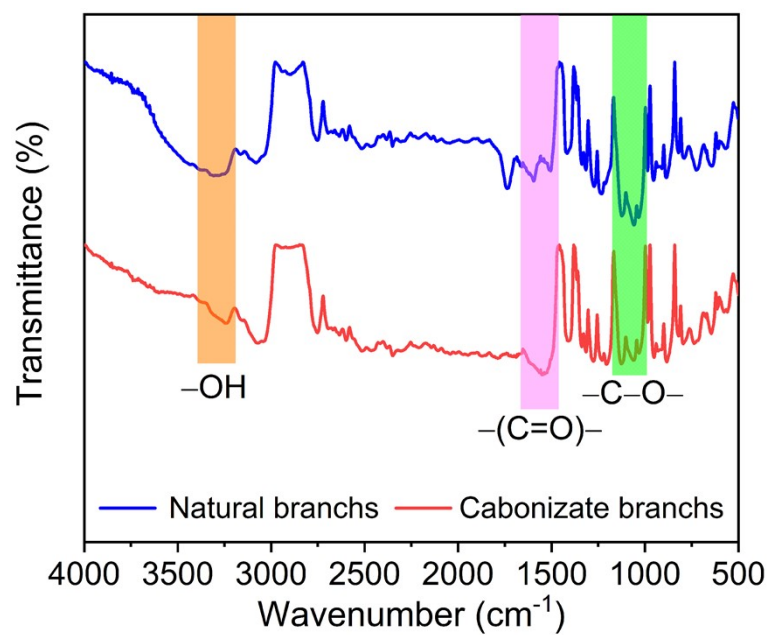
Figure S4. FTIR spectrum of the natural branches and the carbonized branches.

Figure S5. SEM images of the carbonized branches. (a-b) Branch section direction. (c-d) Branch growth direction.

Figure S6. Digital photos of the evaporator surface after long-term evaporation in 3.5wt% NaCl solution.

Figure S7. The efficiency of ordinary and SR-3mm evaporators in a 20wt% NaCl solution under 1 sun irradiation.

Figure S8. The computational domain used in the CFD simulation to determine solute diffusion through the structure of different photothermal materials (PTMs).
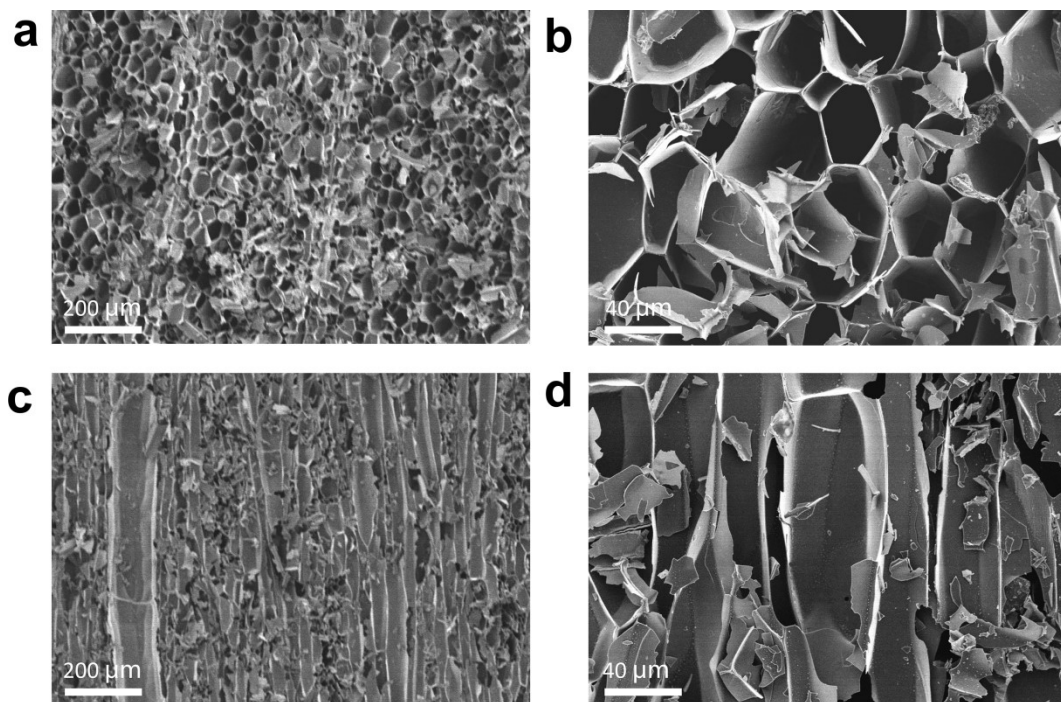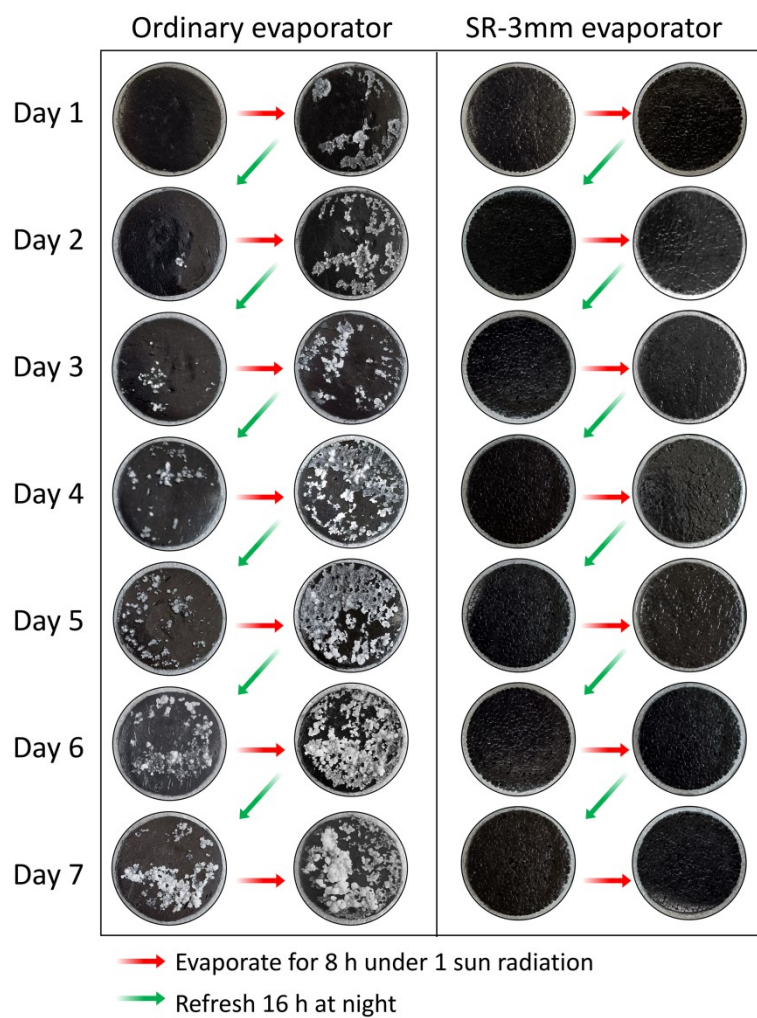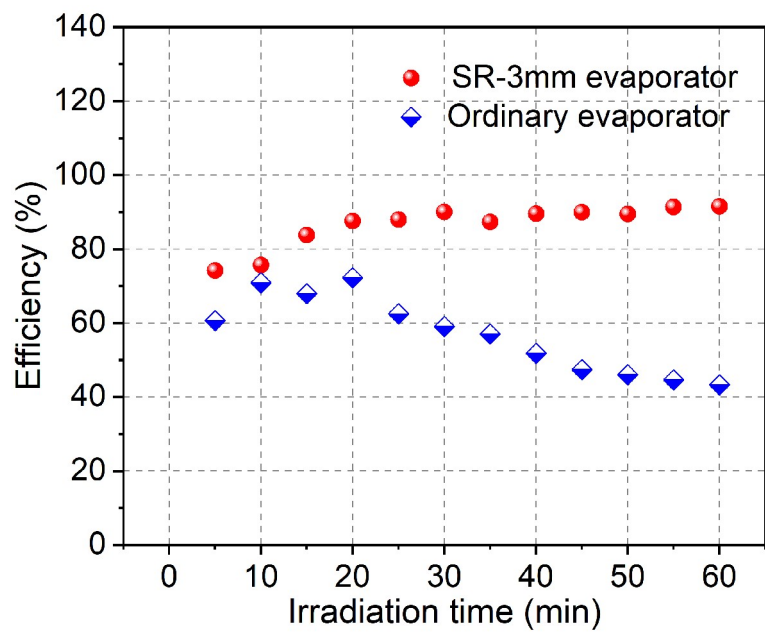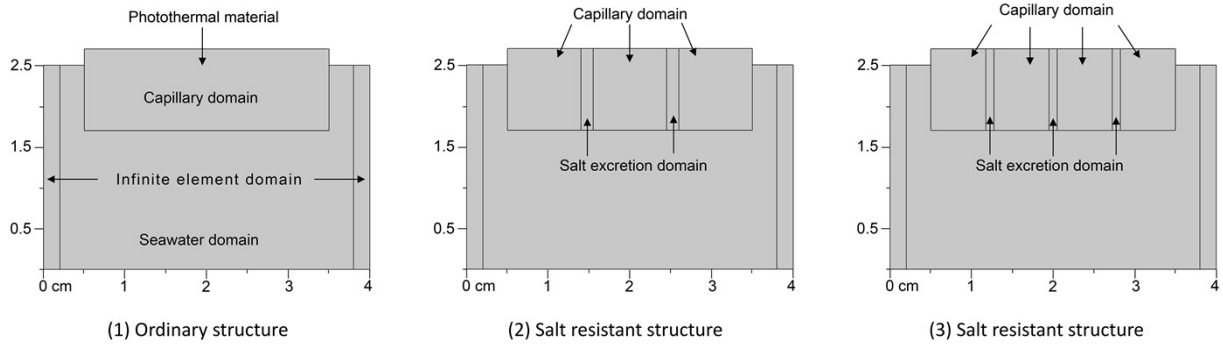
Computational Fluid Dynamics (CFD) modeling: Solute Diffusion. COMSOL multiphysics software was used to understand the diffusion of solute in PTMs with different internal structures. This process is mainly to reflect the transportation of concentrated brine generated after photothermal evaporation within the PTMs. Three solute diffusion systems constructed of PTMs with different internal structures were simulated. First, a porous media domain with a height of 10 mm was constructed to represent the PTMs, and the PTMs was exposed 2 mm above the horizontal plane. Secondly, a infinite element domain is designed for seawater domain to simulate the boundless ocean, mainly to offset the influence of the boundary of seawater domain on solute diffusion. The main difference: 1: the PTMs in the ordinary structure (1) is entirely composed of capillary domains. 2: The PTMs in the SR structure (2) consists of a capillary domain and a salt excretion domain. 3: The capillary and salt excretion domains in the SR structure (2 and 3) are of the same size. The specific solute diffusion system is described as follows:

Richards' equation governs the saturated-unsaturated flow of water in the porous media (Ref. 1-2). We assume that pressure changes in air do not affect the flow and use Richards' equation here for the simulation.

$$(C + S_eS)(\P H_p/\P t) + \nabla \cdot (-K\nabla(H_p + D)) = 0 \tag{1}$$

where C denotes specific moisture capacity (m^{-1}); S_e is the effective saturation of the porous media (dimensionless); S is a storage coefficient (m^{-1}); H_p is the pressure head (m), which is proportional to the dependent variable, p (Pa); t is time; K equals the hydraulic conductivity (m s^{-1}); D is the direction that represents vertical elevation (m).

To be able to combine boundary conditions and sources with the Darcy's Law formulation,

COMSOL Multiphysics converts Richards' equation to SI units and solves for the pressure (SI unit: Pa). Hydraulic head, $\mathbf{H}$, pressure head, H_p, and elevation $\mathbf{D}$ are related to pressure p as：

$$H_p = p/\rho g \; ; H = H_p + D \tag{2}$$

Also, the permeability $\boldsymbol{\kappa}$ (SI unit: m^2) and hydraulic conductivity K (SI unit: m s^{-1}) are related to the viscosity $\boldsymbol{\mu}$ (SI unit: Pa·s) and density $\boldsymbol{\rho}$ (SI unit: kg m^{-3}) of the fluid, and the acceleration of gravity $\mathbf{g}$ (SI unit: m s^{-2}) by

$$\kappa/\mu = K/\rho g \tag{3}$$

In here,

$$S = (\theta_s - \theta_r)/(1 \text{ m} \cdot \rho g) \tag{4}$$

where $\boldsymbol{\theta_s}$ and $\boldsymbol{\theta_r}$ denote the volume fraction of fluid at saturation and after drainage, respectively. With variably saturated flow, fluid moves through but may or may not completely fill the pores in the PTMs, and $\boldsymbol{\theta}$ denotes the volume fraction of fluid within the PTMs. The coefficients C, $\mathbf{Se}$, and K vary with the pressure head, H_p, and with $\boldsymbol{\theta}$, making Richards' equation nonlinear.

Furthermore, K is a function that defines how readily the porous media transmits fluid. The relative permeability of the porous media, k_r, increases with fluid content giving $K = K_s k_r$, where K_s (m d^{-1}) is the constant hydraulic conductivity at saturation. This model uses predefined interfaces for van Genuchten formulas (Ref. 3) to represent how the four retention and permeability properties — $\boldsymbol{\theta}$, C, S_e, and $k_r = K/K_s$ — vary with the solution H_p.

Transport of diluted species in porous media: Fluid flow and solute transport are linked by fluid velocities. With the form of the transport equation that follows, the fluid velocities need to come from Darcy's law:

$$\mathbf{u} = K_s k_r \nabla(H_p + D) \tag{5}$$

In this expression, $\mathbf{u}$ is Darcy's velocity field (SI unit: m s^{-1}). The equation that governs advection, dispersion, sorption, and decay of solutes in fluid is

$$(\partial/\partial t)(\theta c) + (\partial/\partial t)(\rho_b c_p) + \mathbf{u} \cdot \nabla c + \nabla \cdot (-\theta D_L \nabla c) = \sum R_L + \sum R_P + S_c \tag{6}$$

It describes time rate of change in two terms: c denotes dissolved concentration (mol m^{-3}), and $\mathbf{c_P}$ is the mass of adsorbed solute per dry unit weight of PTMs (mg kg^{-1}). Further, $\boldsymbol{\theta}$ denotes the volume fluid fraction (porosity), and $\boldsymbol{\rho_b}$ is the bulk density (kg m^{-3}). In the equation, $\mathbf{D_L}$ is the hydrodynamic dispersion tensor (m^2 d^{-1}); $\mathbf{R_L}$ represents reactions in water (mol (m^3·d)$^{-1}$); and $\mathbf{R_P}$ equals reactions

involving solutes attached to the porous media (mol (m³·d)⁻¹). Finally, S_c is solute added per unit volume of porous media per unit time.

It is far more convenient to solve the above equation only for dissolved concentration. This requires expanding the left-hand side to

$$(\partial/\partial t)(\theta c) + (\partial/\partial t)(\rho_b c_p) = \theta(\partial c/\partial t) + c(\partial\theta/\partial t) + \rho_b(\partial c_p/\partial c)(\partial\theta/\partial t) \tag{7}$$

and inserting a few definitions. In this model, solute mass per solid mass, c_P, relates to dissolved concentration, c, through a linear isotherm or partition coefficient k_P (m³ kg⁻¹) where $c_P = k_P c$. Because the relationship is linear, the derivative is $k_P = \partial c_P/\partial c$. The following substitutions were made to address the solute transport problem.

$$(\theta + \rho_b k_P)(\partial c/\partial t) + c(\partial\theta/\partial t) + \mathbf{u}\cdot\nabla c + \nabla\cdot(-\theta D_L \nabla c) = \theta\Phi_L c + \rho_b k_P \Phi_P c + S_c \tag{8}$$

In the equation, Φ_L and Φ_P denote the decay rates for the dissolved and adsorbed solute concentrations, respectively.

Select the *Time change in pressure head* option for *Fluid fraction time change* in the *Saturation* settings for the *Partially Saturated Porous Media* feature to employ results from the flow equation in the solute-transport model:

$$c(\partial\theta/\partial t) = cC(\partial H_p/\partial t) \tag{9}$$

Note that COMSOL Multiphysics solves for pressure, p, and converts to H_p based on the fluid weight.

MODEL DATA:

The following table provides data for the fluid-flow model:

Variable	Unit	Description	Value 1	Value 2
θ_r	-	Residual saturation	0.001	0.001
α	m⁻¹	Alpha parameter	1.74	1.39
n	-	*n* parameter	1.38	1.6
m	-	*m* parameter	1-1/n	1-1/n
l	-	Pore connectivity parameter	n/a	-
H_{p0}	m	Pressure head	0.01	-
$H_{p0,init}$	m	Initial pressure head	-(y+1.2)-0.2(y+0.4)	-(y+1.2)

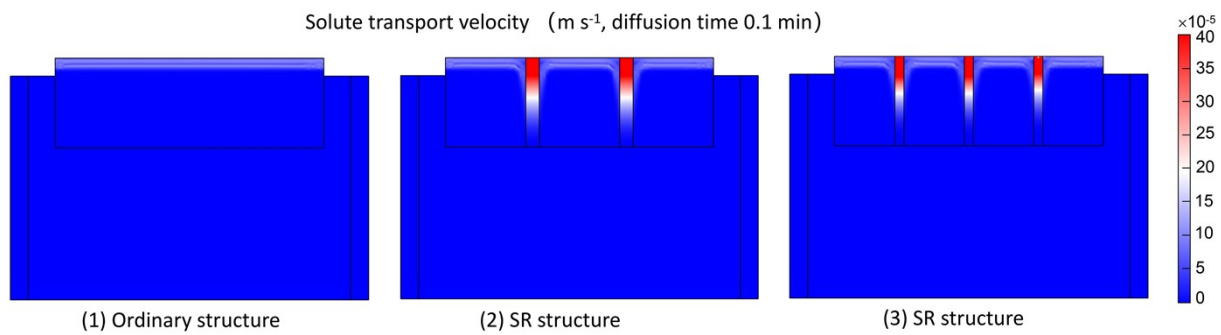| α_y	m	Longitudinal dispersivity	0.005	-
α_x	m	Transverse dispersivity	0.001	-
DI	$m^2 \, s^{-1}$	Diffusion coefficient of NaCl	$1.99e^{-9}$	-
c_0	$mol \, L^{-1}$	Solute concentration	6.14	-
H	m	Initial concentration pressure head	0.01	-

Figure S9. Distribution of solute transport velocity for PTMs with different structures.
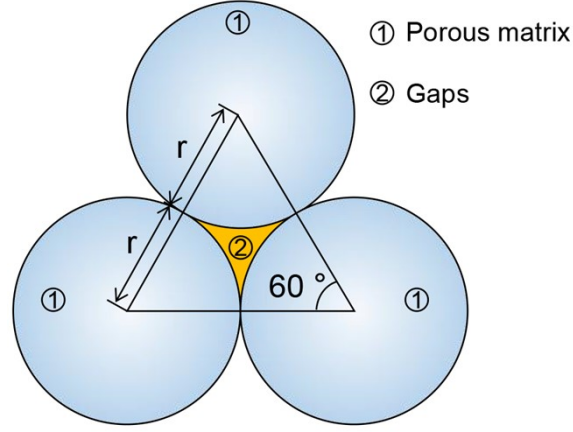
Figure S10. Schematic illustration of the gap created by the assembly of microstructural units. The hydraulic conductivity in the gap can be estimated by the Hagen–Poiseuille law (Equation 10).

$$Q = \frac{\pi G r^4}{8\mu}$$

(10)

where Q is the hydraulic conductivity, G the ratio of the pressure gradient across the length of the pipe, r the pipe radius, and μ the luid viscosity. After normalizing the area of the gap, the radius r_g of the gap channel can be analogized. The area of the gap (S_g) can be calculated by Equation 11.

$$S_g = r_1^2\left(\sqrt{3} - \frac{\pi}{2}\right)$$

(11)

After normalization, the radius of the gap (r_g) can be expressed by Equation 12.

$$r_g = \sqrt{\frac{r_1^2\left(\sqrt{3} - \frac{\pi}{2}\right)}{\pi}}$$

(12)

where r_1 is the radius of the microstructural unit. It can be seen from Figure S5 that the pore radius of the porous matrix is ~20 μm. The microstructural unit radius (r_1) is 1.5 mm in SR-3mm evaporators. Therefore, according to the above formula, the hydraulic conductivity of the gaps exceeds ~83,000 times that of the pores in the porous matrix.
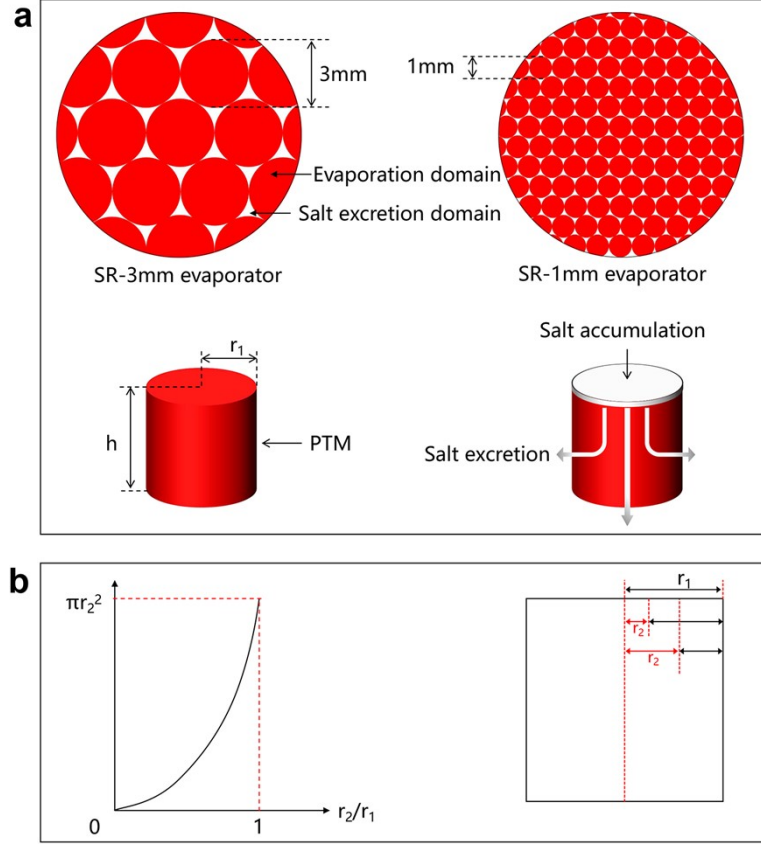
Figure S11. Specification characteristics of PTMs with SR structure. (a) Variation in size and gap of microstructured units. (b) The effect of changes in unit radius on the evaporation area and its advective diffusion paths.

It can be clearly seen from the above figure that there are at most 6 gaps around each microstructure unit, and at least 3 microstructure units are required to form each gap. Therefore, in order to generate gaps, the number n of microstructure units needs to satisfy $n \geq 3$. When $n = 3$, the area of the evaporator (S_A) can be expressed as:

$$S_A = S_{eva} + S_{gap} = 3\pi r_1^2 + r_1^2\left(\sqrt{3} - \frac{\pi}{2}\right) = r_1^2\left(\sqrt{3} + \frac{5\pi}{2}\right)$$

(13)

The ratio of the gap to the evaporator area is:

$$\frac{S_{gap}}{S_A} = \frac{r_1^2\left(\sqrt{3} - \frac{\pi}{2}\right)}{r_1^2\left(\sqrt{3} + \frac{5\pi}{2}\right)} = \frac{\sqrt{3} - \frac{\pi}{2}}{\sqrt{3} + \frac{5\pi}{2}}$$

(14)

When $n > 3$, each microstructural unit in the outermost layer cannot generate six gaps. But when n is close to infinity, ignoring the outermost microstructure unit, each microstructure unit can match two

gaps, and the evaporator area can be expressed as:

$$S_A = nS_{eva} + 2nS_{gap} = n\pi r_1^2 + 2nr_1^2\left(\sqrt{3} - \frac{\pi}{2}\right) = 2\sqrt{3}nr_1^2 \tag{15}$$

The ratio of the gap to the evaporator area is:

$$\frac{2S_{gap}}{S_A} = \frac{2nr_1^2\left(\sqrt{3} - \frac{\pi}{2}\right)}{2nr_1^2\sqrt{3}} = 1 - \frac{\pi}{2\sqrt{3}} \tag{16}$$

Equations 14 and 16 show that the ratio of the gap to the evaporator area is constant regardless of the n and r_1 of the microstructured elements.

Although r_1 does not change the total area of the gaps, it causes an increase in the number of gaps. Since the advective transport of salt ions requires diffusion through the sides of the microstructural unit, changes in the sides area of the microstructural unit (S_{side}) have a strong effect on the salt tolerance of the system.

$$S_{side} = 2n\pi h r_1 \tag{17}$$

where h is the height of the microstructural unit.

The excretion of salt ions is mainly divided into two processes, the first is the diffusion inside the PTMs (microstructural units), and the second is the diffusion in the gap. Due to the extremely high hydraulic conductivity of the gap, the salt discharge capacity of the system mainly depends on the first-step diffusion of salt ions inside the PTMs to the gap.

In the steady state condition, for the diffusive system, the salt conservation equation is:

$$S_{eva}m_{eva}c_{in} = \frac{S_d D_{NaCl}\rho_{eva}(c_{eva} - c_{in})}{l_{length}} \tag{18}$$

where D_{NaCl} is the diffusion coefficient (m^2 s^{-1}) of NaCl in water, and m_{eva} is the steady state evaporation rate (kg m^{-2} h^{-1}), c_{in} is the brine mass fraction initially entering the evaporator (wt%), and the c_{eva} is local mass fraction of salt on the evaporation surface. S_d is the area where salt ion excretion occurs. The ρ_{eva} is the average partial density of water in the diffusion domain, can be calculated according to the following formula.

$$\rho_{eva} = \frac{w_{wet} - w_{dry}}{\dfrac{(w_{wet} - w_{dry})}{\rho_{water}} + \dfrac{w_{dry}}{\rho_{d-d}}} \tag{19}$$

where w_{wet} is the wet weight of the diffusion domain after sufficient water absorption and w_{dry} is the weight of the diffusion domain in dry conditions. ρ_{water} is the density of water and ρ_{d-d} is the density of diffusion domain. l_{length} is the effective diffusion distance of salt ions.

The left hand side of the salt conservation equation is the salt accumulation rate on the absorber and the right hand side is the diffusion rate downward. After the salt gradient rearrangement, the diffusion path of the original salt ions from the evaporator surface to the bottom bulk seawater is changed to a path from the evaporator surface to the side gap. When salt ions are mainly excreted from the gap, the area where salt transfer occurs is mainly the side of the microstructure unit. The diffusion of salt ions in the microstructural unit is not uniform, and the path length of the diffusion is exponentially related to the amount of accumulated salt (**Figure S11b**). The resulting salt diffusion path for any radius r_2 in a microstructural unit of radius r_1 can be integrated by the following equation.

$$l_{length} = \int_0^{r_1} (r_1 - r_2)d2\pi r_2 \tag{20}$$

Therefore, the salt conservation equation can be expressed as:

$$S_{eva}m_{eva}c_{in} = \frac{S_{side}D_{NaCl}\rho_{eva}(c_{eva} - c_{in})}{\int_0^{r_1} (r_1 - r_2)d2\pi r_2} \tag{21}$$

After substituting the constant term into the simplification, for the radius of the microstructural unit one can write:

$$r_1 = \sqrt[3]{\frac{D_{NaCl}\rho_{eva}(c_{eva} - c_{in})2h}{\pi m_{eva}c_{in}}} \tag{22}$$

For this experiment, the SR evaporator constructed from microstructural units derived from balsa branches can adjust the diameter of branches according to different brine salinities. For example, when D_{NaCl} is 1.99×10^{-9} m² s⁻¹, ρ_{eva} is ~0.85 kg m⁻³, and the highest salinity of the evaporator surface (c_{eva}) is 26.79wt% at 40 °C, the theoretically calculated diameter of the microstructural unit for processing 20wt% brine is ~4.3 mm, which requires the construction of an SR-4.3mm evaporator. When processing brine up to 25wt%, the theory requires the construction of an SR-2.64mm

evaporator, which matches the performance of the SR-3mm evaporator tested in this experiment. The bias comes from multiple sources, such as the inevitable inherent differences in the natural branches used in the experiments, and the calculated diameters are the result of statistics. Another part of the transfer of salt ions can be diffused through the bottom surface, which is ignored in the calculation.
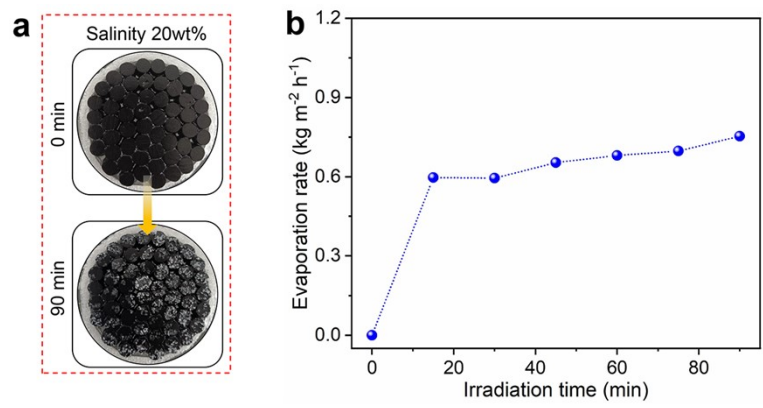
Figure S12. Evaporation performance of SR-6mm evaporator in brine with 20wt% salinity under 1 sun. (a) Photo of surface salt accumulation on evaporator. (b) Evaporator steam generation performance.
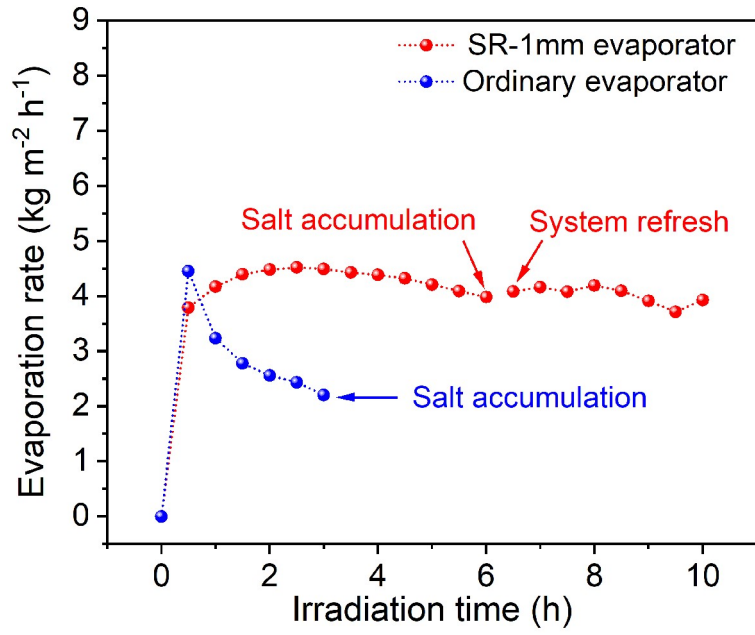
Figure S13. Evaporation, accumulation-salt and refresh performance of SR evaporators in supersaturated brine under 5 sun irradiation.
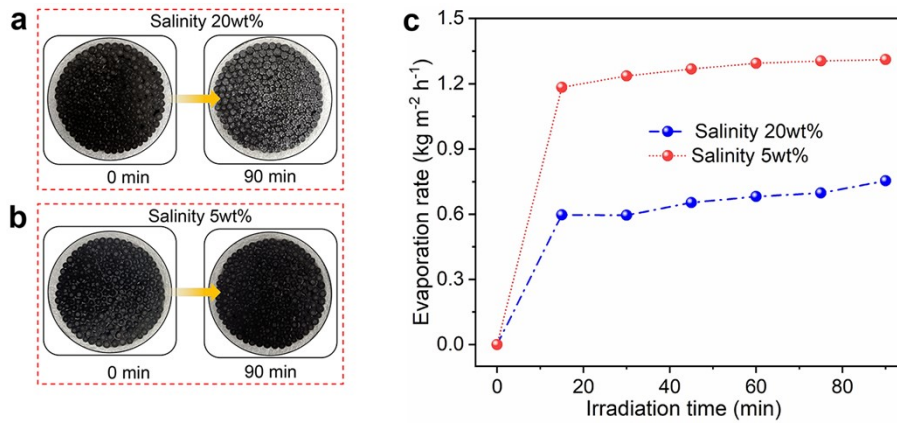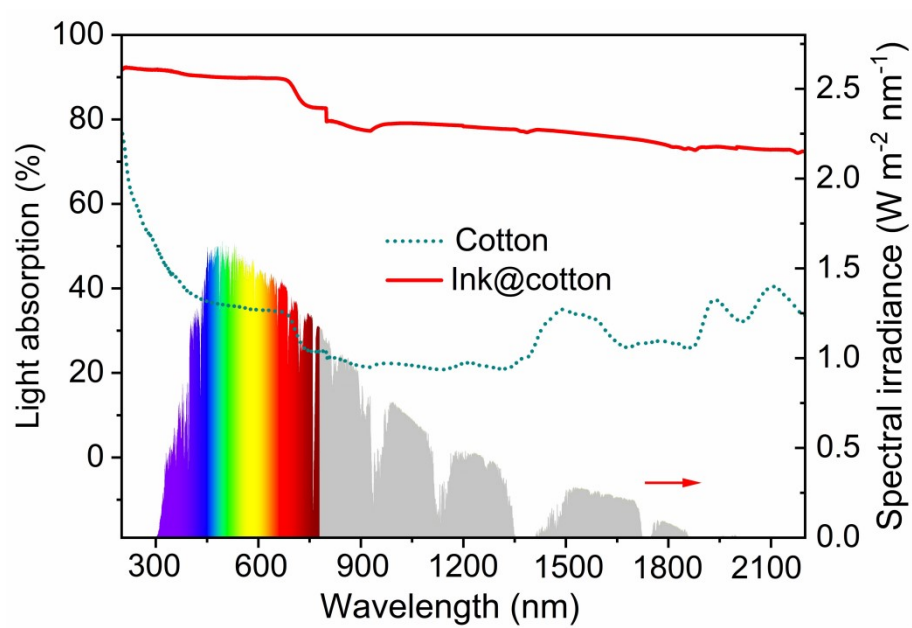
Figure S14. Evaporation performance of SR-3mm (willow) evaporator in brine with 5wt% and 20wt% salinity under 1 sun. (a) Photo of surface salt accumulation on evaporator. (b) Evaporator steam generation performance.

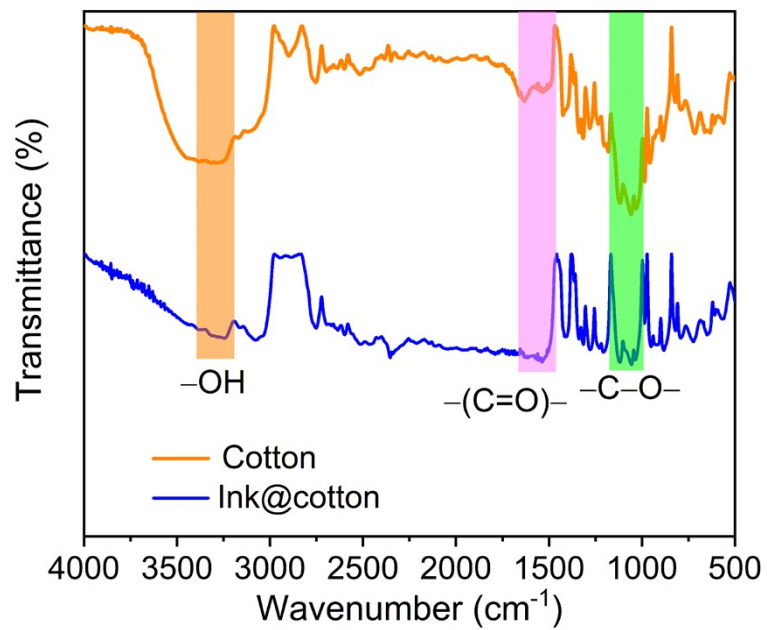**Figure S15.** UV-vis-NIR absorption spectra of the natural cotton and ink@cotton.

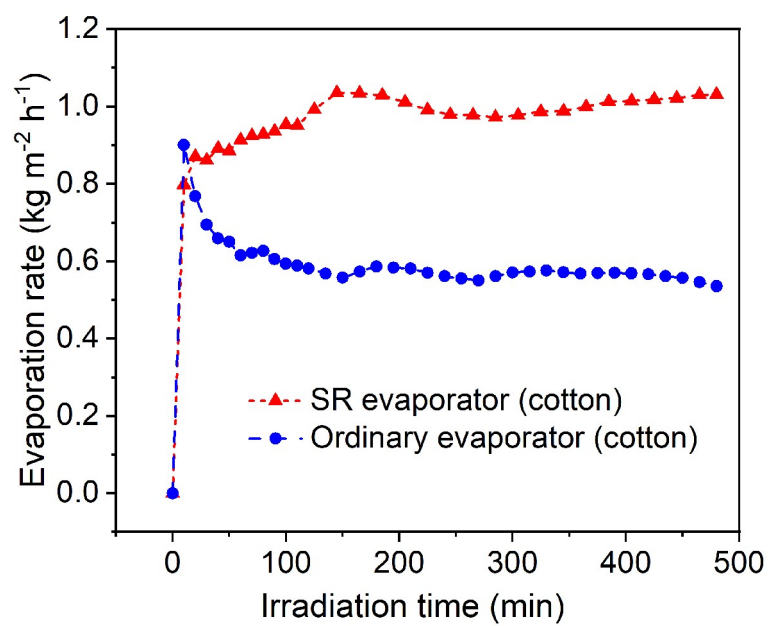**Figure S16.** FTIR spectrum of the natural cotton and ink@cotton.

Figure S17. Evaporation rate of the SR evaporator (cotton) and ordinary evaporator (cotton)
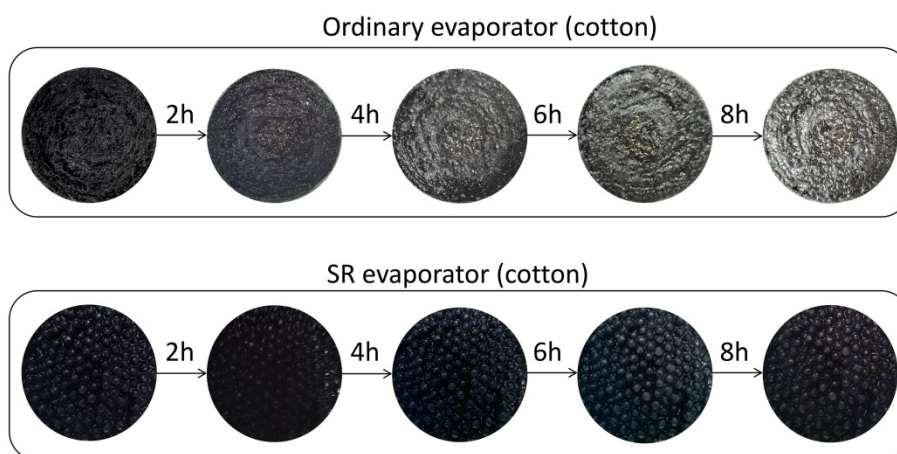
operating in 25wt% brine under 1 sun.

Ordinary evaporator (cotton)

SR evaporator (cotton)

Figure S18. Optical image of the SR evaporator (cotton) and ordinary evaporator (cotton) operating in 25wt% brine under 1 sun.
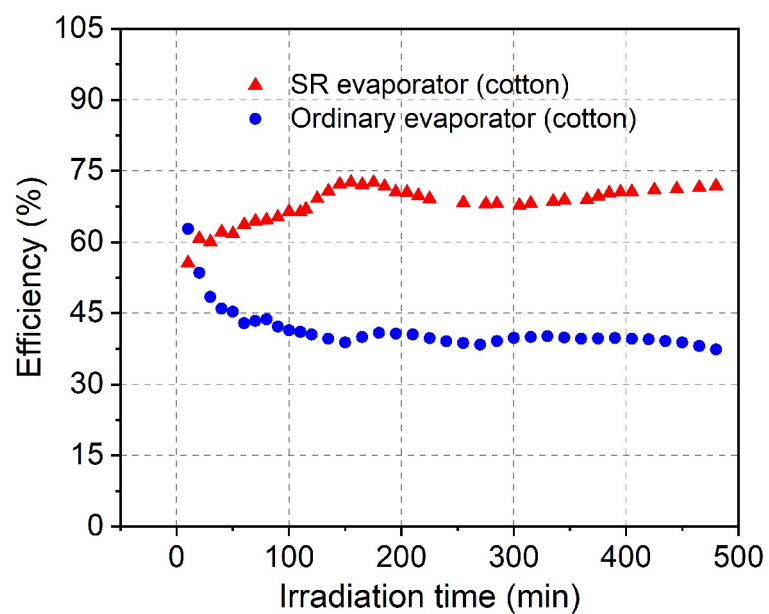
Figure S19. Photothermal efficiency of the SR evaporator (cotton) and ordinary evaporator (cotton) operating in 25wt% brine under 1 sun.
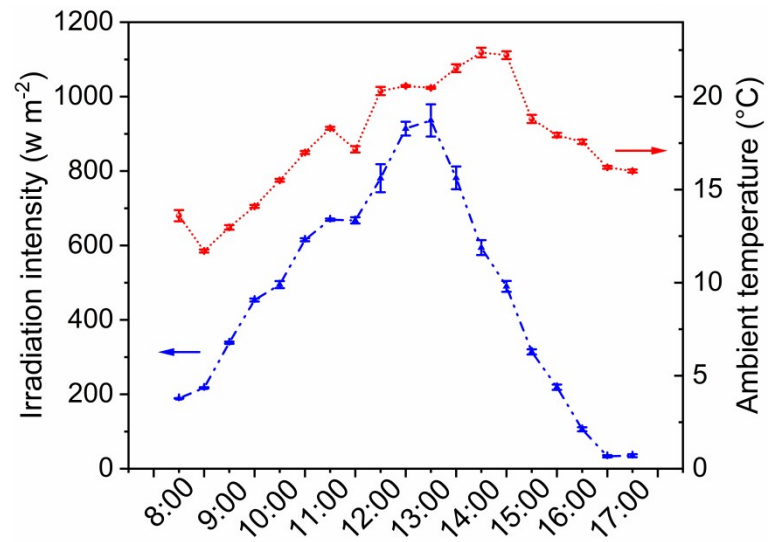
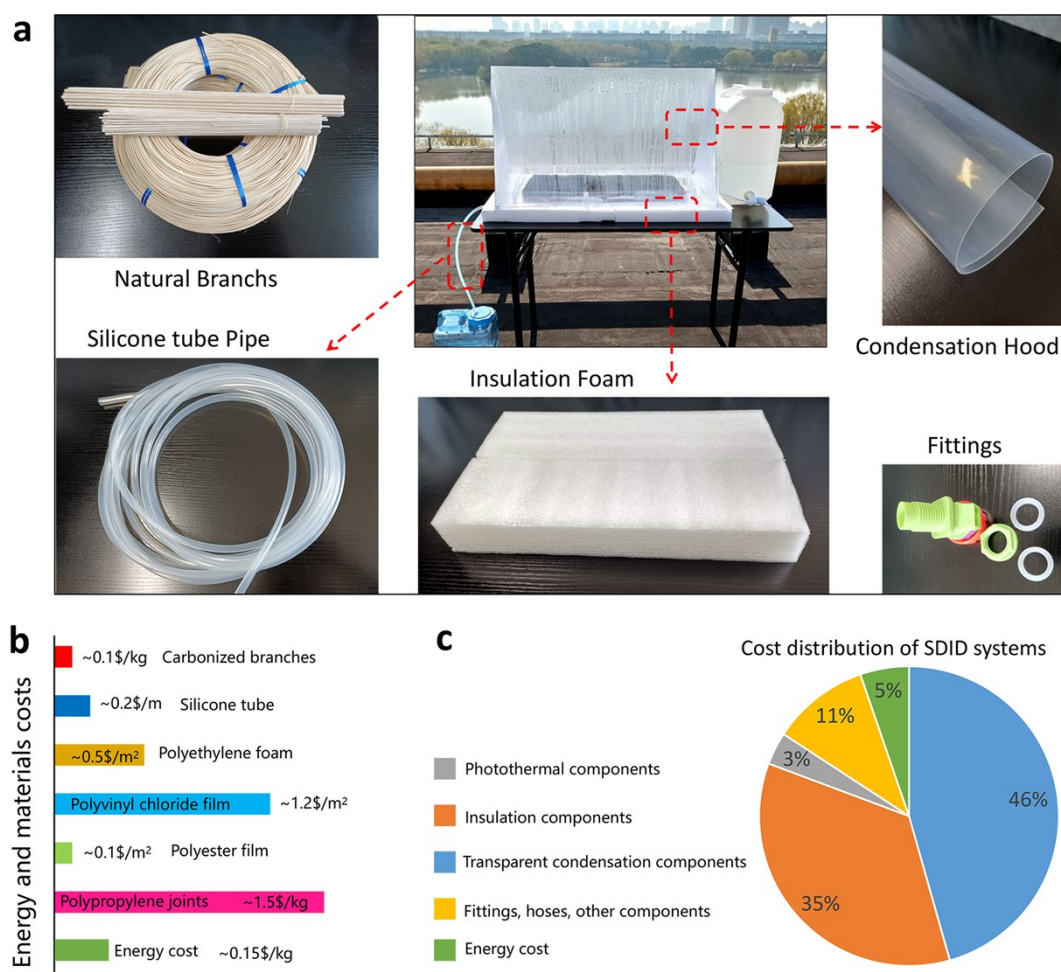**Figure S20.** Outdoor real-time light intensity and temperature changes.

Figure S21. Bill of materials for SDID system. (a) Basic components of SDID system. **(b)** Material species of SDID system. **(c)** Cost distribution of SDID system.

The materials list includes the natural branches (Basa tree, vine), polypropylene connectors, 0.4 mm thick clear polyvinyl chloride film (Tongshi), silicone tube (Audrey Xin,) and expanded low density polyethylene (thickness 5cm). The cost of each part is summarized below using prices of similar items found on Alibaba.com. From this estimate, the material cost of the floating solar evaporator is around ~$1.8-3 per square meter of solar evaporator, the cost is extraordinarily low.

References

1. J. Simunek, T. Vogel, and M.Th. van Genuchten, The SWMS_2D code for simulating water flow and solute transport in two-dimensional variably saturated media, ver. 1.1., *U.S. Salinity Laboratory, USDA,* 1994, Research Report No. 132.
2. J. Bear, *Hydraulics of Groundwater*, McGraw-Hill, 1978.
3. M.Th. van Genuchten, A closed-form equation for predicting the hydraulic of conductivity of unsaturated soils, *Soil Sci. Soc. Am. J.*, 1980, **44**, 892–898, .